ACS OMEGA

Open Access

http://pubs.acs.org/journal/acsodf

Article

A Comprehensive Study on the Effect of Highly Thermally Conductive Fillers on Improving the Properties of SBR/BR-Filled Nano-Silicon Nitride

Sajad Rasouli, Amirreza Zabihi, Mohammad Fasihi,* and Gholamreza Bozorg Panah Kharat

Cite This: *ACS Omega* 2023, 8, 32701−32711

Read Online

ACCESS | Metrics & More | Article Recommendations

ABSTRACT: The effect of silicon nitride (Si_3N_4) as a thermally conductive material on the mechanical, microstructural, and physical properties as well as kinetics of the curing reaction of styrene-butadiene rubber/butadiene rubber (SBR/BR) was investigated in this work. The results showed an improvement in tensile, hardness, and compression features of the composite due to the presence of Si_3N_4. The properties were enhanced with the filler loading content; somehow, the composite including Si_3N_4 = 6 parts per hundred (phr) had the most significant performance, an increase of ∼15 and 20% in the maximum strain and toughness of the composite, respectively, an increase of almost 7% in the hardness, and an ∼13% reduction in the compression set. Also, the filler led to an increase in the crosslink density (calculated via the Flory−Rehner equation using swelling test) by 7.12 × 10^{-5} mol/g, proving the increment of the covalent bonds between the polymer chains during the curing reaction. The kinetic consideration revealed a reduction in the scorch and optimum curing times by ∼40 and ∼25%, respectively. In order to describe the kinetics of curing reaction of SBR/BR-Si_3N_4, an autocatalytic model based on the Kamal−Sourour model was applied on the rheometry results. The calculated kinetic parameters indicated that the thermally conductive Si_3N_4 accelerated the curing reaction by ∼40%, particularly at Si_3N_4 = 6 phr. After 6 phr of Si_3N_4, agglomeration of the filler particles decreased its performance.

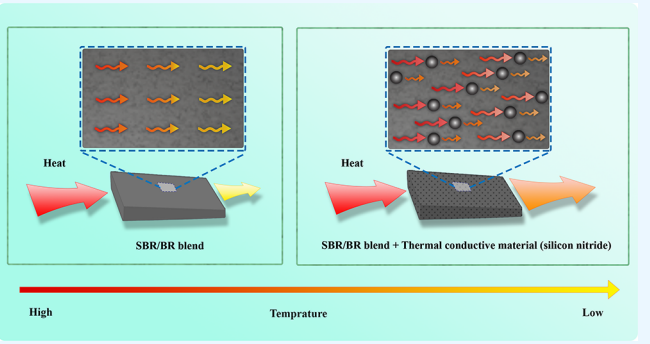

1. INTRODUCTION

Nowadays, rubber has been playing a key role in the car, food packaging, medical, and aerospace industrial fields.[1] Natural rubber (NR),[2] styrene-butadiene rubber (SBR),[3] butyl rubber (PIB),[4] nitrile rubber (NBR),[5] neoprene rubber (CR),[6] and silicon rubber[7] are just a few examples of industrial elastomers that have been used in the aforementioned industries.[8] Impermeability to both water and air,[9] great resistance to chemicals[10] and abrasion,[11] tearing and cutting over a wide range of temperature,[12] electrical insulation,[13] and low cost and lightweight[1] have made rubber a fantastic candidate for industries.

Tire manufacturing is one of the most widely known uses of rubber in the automobile industry, which is so important for the welfare of people.[14] Tires are complex products made of various rubbery sections, e.g., crown, tread, gum, beads, inner layers, and side walls, which are usually made of SBR, butadiene rubber (BR), NR, PIB, *etc.*[15] It is estimated that 40−50% of a tire is rubber.[16] Usually, the rubbers of SBR and BR form 60−70% of the rubbery parts of a tire.[17] This is due to their favorable properties, such as hardness and chemical and water resistance.[18] These two rubbers are usually blended to achieve the appropriate rubber properties for optimal tire performance. Polymer scientists have proved that a high SBR loading results in a better-wet skid and traction properties; however, it leads to an increase in the glass transition temperature (T_g), which affects the tire performance at low temperatures.[19] In contrast, increasing the BR content in the blend reduces the T_g amount of the compound.[20] Therefore, the SBR/BR ratio in a typical compound for a car tire should be adjusted to control the T_g value.

In conjunction with the SBR/BR-based composites, some studies have been conducted with respect to their morphology and physicomechanical and thermal properties.[17,20,21] Thermal conductivity is one of the most essential characteristics, which can change the final properties and quality of rubber-based composites.[22] Hence, increasing the rubber heat conductivity

Received: May 21, 2023
Accepted: August 11, 2023
Published: August 29, 2023

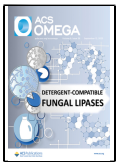

improves the vulcanization process economically and also leads to dissipation of the generated heat in the cured composite under operational conditions, causing the maintenance of the operating temperature at a safe level.[23] Incorporation of thermally conductive inorganic fillers into the rubber matrix is one of the best methods to enhancing the thermal conductivity of rubbers.[24] Silicon carbide,[25] alumina,[26] boron nitride,[27] aluminum nitride,[28] and different types of carbon derivatives[29] as well as hybrid fillers[30] are used as thermally conductive fillers to improve the heat transfer into the polymeric matrix. Silicon nitride (Si_3N_4) with an intrinsic thermal conductivity of ~86−120 W/m·K is a type of ceramic material used for numerous applications due to its high-temperature strength, outstanding thermal shock resistance, low thermal expansion coefficient, and high oxidation resistance.[31,32] Belgacemi et al.[33] investigated the effect of surface-modified Si_3N_4 at different amounts of the filler on the mechanical properties of epoxy composites. They found that the surface modification of Si_3N_4 led to better filler dispersion leading to the improvement of tensile strength, bending, storage modulus, and glass transition temperature features. Tai et al.[34] developed a new surface modification strategy with a macromolecular coupling agent for nano-Si_3N_4 to increase dispersion of the filler in the nonpolar and weak polar rubbery matrixes such as SBR, BR, and NBR. In this regard, Derradji et al.[35] also reported that the onset decomposition temperature and thermal stability of these rubber-based composites were highly improved via adding Si_3N_4. In another study, the addition of 70% nano-Si_3N_4 enhanced the nanocomposite thermal conductivity from 0.18 to 5.78 W/m·K.[36]

So far, few research works have been conducted concerning the improvement of SBR/BR thermal properties while their blend has great importance in the tire industry, particularly tire tread. Moreover, highly thermally conductive materials as filler can provide special performance to the SBR/BR-based composite, especially kinetics of the vulcanization reaction of the compound. The presence of a thermally conductive particle in the composite media improves the thermal diffusivity of the tire compound, which can create a perfect heat transfer within a tire. In addition, the heat transfer prevents the tire explosion while deriving due to the increment of the inside air temperature of the tire, particularly in hot weather. The Si_3N_4 filler has the ability to be a good candidate for these missions. In this research work, we have a keen interest in studying the effect of Si_3N_4 as a highly thermally conductive filler on the SBR/BR-based composites for use in the tire industry. This is because few research works have been unfortunately conducted concerning the improvement of SBR/BR properties so far. In this regard, different nano-Si_3N_4 loading contents are applied to deeply study the influence of Si_3N_4 on the physical, mechanical, and crosslinking degree properties as well as kinetics of the curing reaction of SBR/BR-filled Si_3N_4 composites.

2. MATERIALS AND METHODS

2.1. Materials. SBR type 1500 was purchased from Bandar Imam Petrochemical Co. (Khouzestan, Iran), and BR (high cis, type 1210S) was provided by Shazand Petrochemical Co. (Arak, Iran). The chemicals of zinc oxide (ZnO), stearic acid, sulfur, and paraffin wax were purchased from Arian Tootia Co. (Shahr-e Kord, Iran), Pars Pak Kimiya Co. (Tehran, Iran), Parto Googerd Asia Co. (Tehran, Iran), and Tosan Petro Energy Co. (Tehran, Iran), respectively. Also, antioxidant 4010NA (*N*-isopropyl-*N*′-phenyl-*p*-phenylenediamine) was bought from Rongcheng Chemical General Factory Co., Ltd. (Shandong, China). Accelerator CZ (*N*-cyclohexyl-2-benzothiazolesulfenamide) and accelerator DM (2,2′-dibenzothiazoledisulfde) were provided by Kemai Chemical Co., Ltd. (Tianjin, China). Nano-Si_3N_4 (type US2038) with the purity of 99%, particle size of 30 nm, density of 3.4 g·cm^{-3}, and special surface area of 120 m^2/g was also supplied by US Research Nanomaterials, Inc. (Florida, USA).

2.2. Preparation of SBR/BR-Filled Si_3N_4. In the present work, the compound of SBR/BR-filled Si_3N_4 (SBR/BR-Si_3N_4) was prepared in six steps: pre-blending, batch fusion, masterbatch, resting, final, and forming steps. The steps of pre-blending, masterbatch, and final were implemented by using a lab-scale internal mixer (Brabender Plasticorder). Also, the steps of batch fusion and forming were performed on a lab-scale two-roll mill with the size of 6″ × 12″ (Farrel Pomini). The preparing process of SBR/BR-filled Si_3N_4 is as follows:

(1) In the pre-blending step, the pure SBR and BR with the blend ratio of 65/35 were added to the internal mixer. The fill factor was adjusted to 75% of the maximum load capacity of the mixer. Next, the blend was mixed for 60 s at 50 rpm, as the mastication process. In this step, the temperature controller was fixed at 50 °C. Next, the half of the Si_3N_4 filler and paraffin wax were gently added to the blend for 20 s and mixed for 60 s with the rotor rate of 50 rpm. After a ram sweep for 30 s, and mixing for 60 s, the compound was discharged.

(2) In the batch fusion step, the pre-blended compound was milled on the two-roll mill for 6 min. Then, the compound was discharged and prepared for the masterbatch step.

(3) In the masterbatch step, the sheet compound was poured into the mixer and mixed for 60 s under 50 rpm. After 60 s, the rest of the Si_3N_4 filler and paraffin wax were added to the compound—similar to the conditions of pre-blending step—and mixed for another 60 s. The temperature controller was also set at 50 °C. After a twice ram sweep for 30 s and mixing for 60 s, the compound was discharged.

(4) In the resting step, the masterbatch was led to relax in the ambient temperature for 24 h.

(5) In the final step, the rested masterbatch was poured into the mixer and mixed for 60 s under 50 rpm. Then, the remaining chemicals, i.e., ZnO, antioxidant 4010NA, stearic acid, sulfur, accelerator CA, and DM (according to Table 1) were slowly added to the compound for 30 s. Next, the mixture was mixed for 60 s. After a twice ram sweep for 30 s and mixing for 50 s, the final compound was discharged from the mixer.

(6) In the forming step, the final compound was milled on the two-roll mill and formed for 4 min. At the end, the sheet compound was discharged from the two-roll mill.

It should be mentioned that the two-roll mill apparatus was equipped with the water circulation (with the temperature of 30 °C) for cooling. Also, the maximum temperature at the mixing procedure in the internal mixer was 120 °C. In this work, the aforementioned preparation process was used for all the compounds of SBR/BR-Si_3N_4 with the Si_3N_4 amounts of 0−10 phr (see Table 1).

2.3. Vulcanization of SBR/BR-Si_3N_4. The discharged sheets from the two-roll mill of the sixth step (forming step)

https://doi.org/10.1021/acsomega.3c03548
ACS Omega 2023, 8, 32701−32711

Table 1. Composition of SBR/BR-Filled Si_3N_4 Compounds (in phr[a])

	sample code					
ingredients	S0	S1	S2	S3	S4	S5
SBR	65.0	65.0	65.0	65.0	65.0	65.0
BR	35.0	35.0	35.0	35.0	35.0	35.0
stearic acid	1.1	1.1	1.1	1.1	1.1	1.1
4010NA	2.0	2.0	2.0	2.0	2.0	2.0
ZnO	2	2	2	2	2	2
sulfur	1.85	1.85	1.85	1.85	1.85	1.85
paraffin wax	2.5	2.5	2.5	2.5	2.5	2.5
accelerator CZ	1.0	1.0	1.0	1.0	1.0	1.0
accelerator DM	0.5	0.5	0.5	0.5	0.5	0.5
Si_3N_4	0	2	4	6	8	10

[a]phr: parts per hundred.

were compression molded in a hydraulic hot press at 160 °C and 10 MPa pressure according to their respective cure times. The curing time for each formulation was found by an oscillating disk rheometer (Monsanto ODR 2000, Ohio, USA) at 160 °C. After the curing process, the cured samples were allowed to cool to ambient temperature under the mentioned pressure.

2.4. Testing Performed on SBR/BR-Si_3N_4. *2.4.1. Tension Test.* To perform the tensile test on the cured SBR/BR-Si_3N_4, an Instron 3366 universal testing machine was used according to ASTM D412. Five different dumbbell-shaped samples (for averaging the results) were cut for each formulation using a Wallace die cutter. The tensile test was performed at ambient temperature with the speed of 500 mm/min. The tension test was carried out to obtain the tensile properties, i.e., tensile strength, elongation at break, and tensile modulus of the cured SBR/BR-Si_3N_4.

2.4.2. Scanning Electron Microscopy (SEM). A SEM (TESCAN VEGA II, Czech Republic) image was taken from the cross-section surface of the cured SBR/BR-Si_3N_4 using an accelerating voltage of 30 kV. First, the samples were frozen in liquid nitrogen and then broken followed by vacuum-drying. Before taking the SEM image from the composites, each sample was coated with a thin layer of gold.

2.4.3. Swelling Test. Swelling measurement at room temperature was accomplished according to ASTM D471, in order to determine the crosslinking degree of the cured SBR/BR-Si_3N_4 based on an averaging on the five different samples for each formulation. In the beginning, each sample was cut into the volume of 20 × 20 × 6 mm^3 followed by weighing. Then, all the samples were put into toluene for 48 h. After this period of time, the weight of the swelled samples was again achieved. The crosslinking density is obtained based on the samples' weights after and before 48 h.

2.4.4. Compression Test. The compression test for the cured SBR/BR-Si_3N_4 composites was accomplished according to ASTM D3574. In the beginning, five samples (for averaging the results) with the volume of 50 × 50 × 25 mm^3 were cut for each formulation. Then, the samples were placed between the two plates of the compression machine and compressed to 50% of the original thickness of the samples. Afterward, the samples were subjected to heat with the temperature of 70 °C in a hot-air oven (BIOBASE, model no. HAS-T105, China) for 24 h. In the end, the final thickness of the samples was measured after a recovery for 30 min at ambient temperature. The compression set and recovery percentage were calculated using the space bars and the initial and final thicknesses of the samples.

2.4.5. Density Measurement. The density of the cured SBR/BR-Si_3N_4 was calculated by the buoyancy method using a DM 3000 densimeter (MonTech, Germany) according to ASTM D297. The density was obtained based on an averaging on five different samples for each formulation.

2.4.6. Hardness. The hardness of the SBR/BR-Si_3N_4 samples was determined by Shore A hardness using the Zwick hardness tester according to DIN 53505.

2.4.7. Thermal Diffusivity Measurement. In the present work, the continuous heating method presented by Hands and Horsfall[37] was used to determine the thermal diffusivity of the SBR/BR-Si_3N_4 composites. The technical structure and characteristics of the setup were clearly shown by Goyanes et al.[38] To obtain the thermal diffusivity, the test was repeated five times for each sample and then the final value was calculated based on an average over them.

2.4.8. Rheological Test. Rheological characteristics of the cured SBR/BR-Si_3N_4 samples were obtained using an oscillating disc rheometer (Monsanto ODR 2000, Ohio, USA) according to ASTM D2084. This test was performed to find the cure kinetics, i.e., the minimum torque, maximum torque, curing rate, and optimum cure time, for each sample.

2.5. Theoretical Background of Statistical Analysis. *2.5.1. Kinetics of Vulcanization Reaction of SBR/BR-Si_3N_4.* Using the rheometry test, the kinetics of vulcanization reaction can be obtained by detecting the rheometer torque during the curing reaction of the SBR/BR-Si_3N_4 compound as a function of time. According to the cure data achieved from the torque−time curve, the state of cure or conversion of curing reaction (α) can be calculated using the following equation:[39]

$$\alpha = \frac{M_t - M_L}{M_H - M_L} \tag{1}$$

where M_t is the rheometer torque at time t and the terms of M_L and M_H are the minimum and maximum torques, respectively.

In this work, an empirical kinetic model presented by Kamal−Sourour[40] and modified by Ferasat et al.[41] is used to predict the curing reaction of the SBR/BR-Si_3N_4 compounds. According to this autocatalytic kinetic model, the vulcanization reaction rate ($d\alpha/dt$) during the curing process is defined as follows:[41]

$$\frac{d\alpha}{dt} = \frac{(k_1 + k_2\alpha^m)(1-\alpha)^n}{1 + \exp[C(\alpha - \alpha_c)]} \tag{2}$$

where k_1 and k_2 are the reaction rate constants, which are measurable using the Arrhenius equation;[42] m, n, and C are the model constants as well. The term of α_c indicates the critical conversion.

In the presented kinetic model, the term $(1-\alpha)^n$ illustrates the non-reaction substance.[43] In the rubber curing, the autocatalytic kinetic model is usually used to identify the form of an additional complication of kinetics of the vulcanization reaction via adding the term α^m to the kinetic model.[44] Factually, the parameters of n and m indicate the reaction and autocatalytic reaction orders, respectively.

In the present work, the statistical analysis related to the kinetics of vulcanization reaction of SBR/BR-Si_3N_4 is performed by using the Python programming language.[45]

https://doi.org/10.1021/acsomega.3c03548
ACS Omega 2023, 8, 32701−32711

3. RESULTS AND DISCUSSION

In this work, the obtained results were discussed with respect to the effect of the Si_3N_4 loading content on the mechanical, microstructural, and physical properties as well as the kinetics of the curing reaction of SBR/BR-Si_3N_4. The composite samples were symbolized by S0-S6 containing 0−10 phr of Si_3N_4, respectively.

3.1. Tensile Properties. The stress−strain curves for SBR/BR-Si_3N_4 samples with different amounts of Si_3N_4 resulting from the tensile test are illustrated in Figure 1.

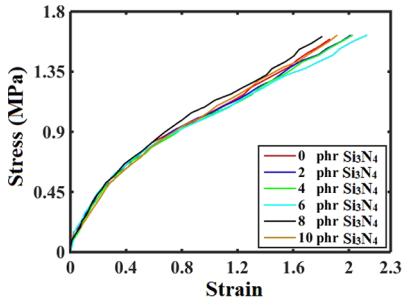

Figure 1. Stress−strain (tensile) curves of SBR/BR-Si_3N_4 samples as a function of the Si_3N_4 loading content.

Using Figure 1, the tensile characteristics, i.e., tensile strength (TS), modulus (E), maximum strain (ε_{max}), and toughness for all the composites were calculated. The mentioned tensile characteristics were achieved according to the following definitions: TS is the maximum load that the composite can support, E is the stress divided by the strain, ε_{max} is the ratio between the changed length and the primary length after breakage, and toughness is the area under the stress−strain curve, respectively. The calculated tensile features for all the samples are reported in Figure 2. To create deep knowledge into the effect of the Si_3N_4 loading content on the tensile characteristics of the SBR/BR-Si_3N_4 composites, each three characteristics were shown in one 3D (three-dimensional) figure. The 3D curves of TS−E−ε_{max} and toughness−ε_{max}−TS as a function of the Si_3N_4 content are shown in Figure 2a and b, respectively.

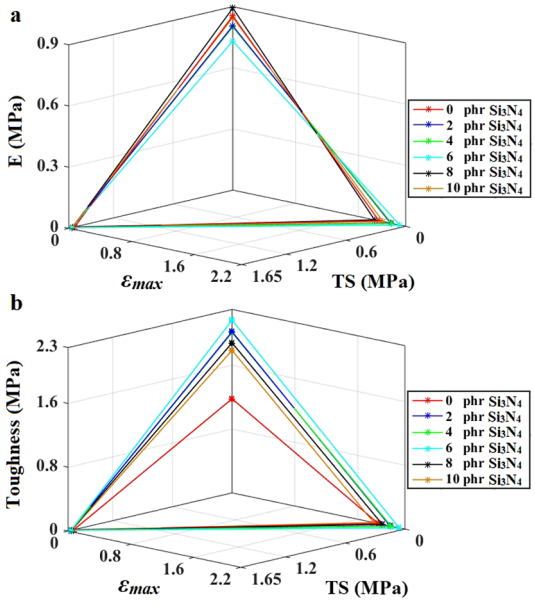

Figure 2. Three-dimensional figures of (a) tensile strength (TS)−modulus (E)−maximum strain (ε_{max}) and (b) toughness−tensile strength (TS)−maximum strain (ε_{max}) as a function of Si_3N_4 loading content.

As seen in Figure 2a, the increment of the Si_3N_4 loading content led to an enhancement of the TS and ε_{max} values, and after the filler amount of 6 phr, the trend was changed to descendant. Therefore, the SBR/BR-Si_3N_4 composite containing 6 phr of Si_3N_4 improved the tensile properties of the composite more than the other formulations. According to Figure 2a, the presence of the Si_3N_4 filler in the recipe reduced the modulus of the composite down to 0.731 MPa at the filler amount of 6 phr and, after that, the trend was changed to ascending. In fact, the Si_3N_4 amount lower than 8 phr improved the elasticity of the composite, which is desirable in the tire industry. In addition, the same variation trend of the tensile characteristics is also observed in Figure 2b. As shown in Figure 2b, the toughness of the composites was raised with the Si_3N_4 content and the trend was changed after the filler amount of 6 phr. However, the composite containing Si_3N_4 had a higher toughness than the pure blend, particularly at 6 phr of Si_3N_4. According to the resultant data, the highly thermally conductive Si_3N_4 with the content of 6 phr leads to the increment of the TS, ε_{max}, and toughness values of SBR/BR-Si_3N_4 to ∼2, 15, and 20% more than the pure blend, respectively. As seen, the used filler had a least effect on the TS of the composite while the toughness was changed 1.2 times the pure blend. Also, the optimum amount of Si_3N_4 (6 phr) reduced the modulus of the composite by 15%. Despite the fact that the presence of Si_3N_4 in the composite as a filler improved the tensile properties, further increment of it reduced the composite tensile characteristics. It can be attributed to the particle agglomeration of the filler. This phenomenon can be affected by the impact of the filler on the thermal conductivity of the compound during the curing process followed by the crosslinking degree of the cured composite. According to the results, it seems that the SBR/BR-Si_3N_4 composite including 6 phr of Si_3N_4 is a good candidate from the mechanical point of view for tire tread. This is because this amount of the filler increases elasticity of the composite while improving its properties.

3.2. Microstructural Properties. A SEM image was taken from the cross section of the fractured samples after the breakage in the tensile test to observe the microstructure and Si_3N_4 agglomeration in the SBR/BR-Si_3N_4 composites. The SEM images for all the samples are illustrated in Figure 3.

As seen in Figure 3, the enhancement of the filler loading content in the composite caused the agglomeration of Si_3N_4 particles and increased their dimensions to larger sizes. According to the SEM images with the 2.0 kx magnification, the agglomeration was more severe after 6 phr of the filler. This issue decreases the performance of the filler in the composite. According to Figures 2 and 3, the good particle size and optimum amount of Si_3N_4 were the main factors in the improvement of the tensile properties of SBR/BR-Si_3N_4 with the filler content of 6 phr. This amount of the filler due to the creation of better heat distribution into the composite matrix can probably increase the crosslinking degree of the composite. To prove this hypothesis, the mentioned characteristic of the samples should be determined.

3.3. Crosslink Density. Crosslink density is very important in the quantification of vulcanization degree of elastomers.[43]

https://doi.org/10.1021/acsomega.3c03548
ACS Omega 2023, 8, 32701−32711

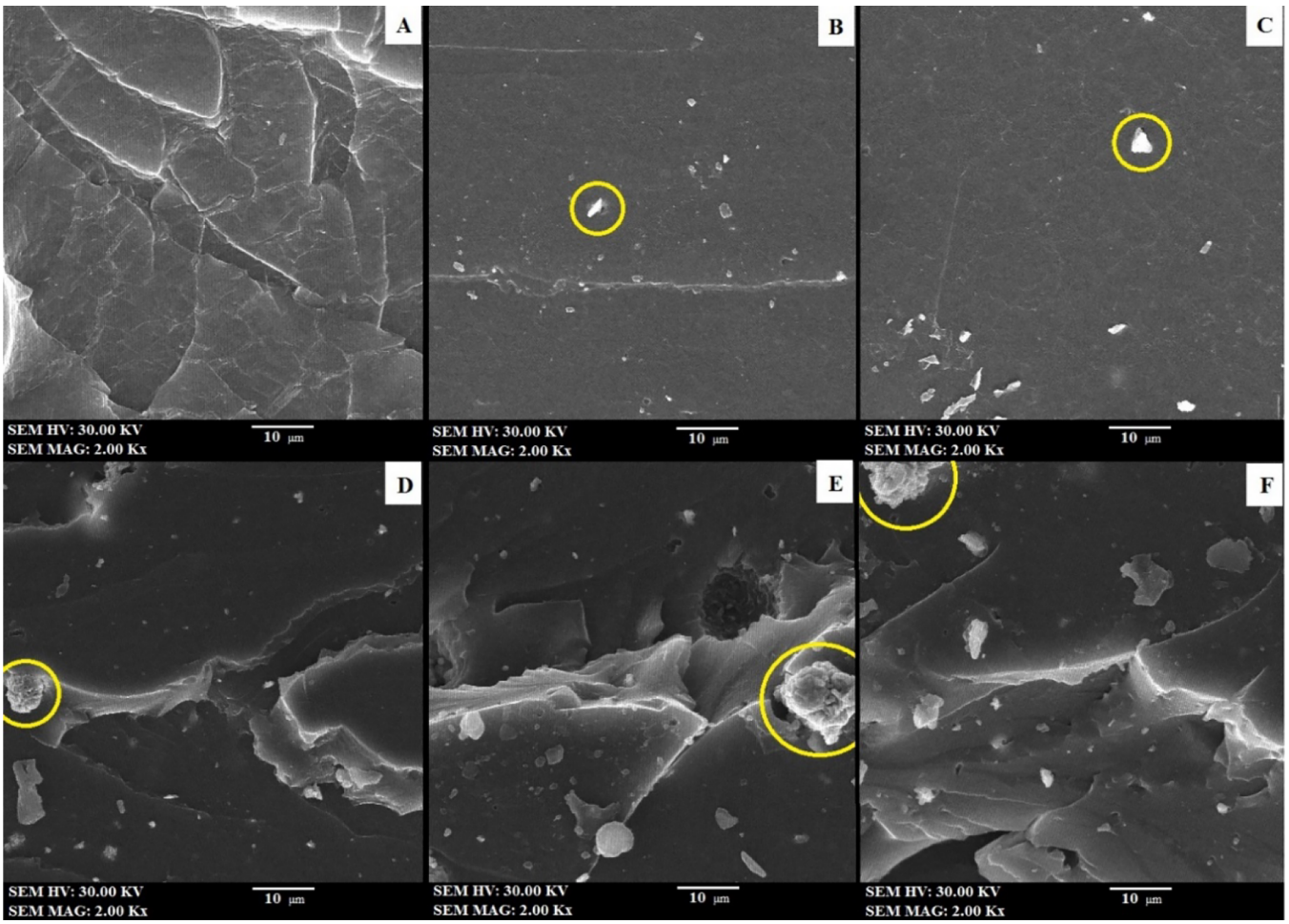

Figure 3. SEM images taken from the cross section of the fractured samples in the tensile test for the SBR/BR-Si_3N_4 composites with the Si_3N_4 contents of (A) 0, (B) 2, (C) 4, (D) 6, (E) 8, and (F) 10 phr. The particle inside the yellow circle is Si_3N_4.

Most of the SBR/BR-Si_3N_4 characteristics are strongly dependent on the crosslinking degree of the composite.[44] The crosslink density of the SBR/BR-Si_3N_4 composites with different loading contents of Si_3N_4 is calculated using the swelling method according to the Flory–Rehner equation (FR) as follows:[46,47]

$$V_p = \frac{\left(\frac{m_i - m_f}{\rho_p}\right)}{\left(\frac{m_i - m_f}{\rho_p}\right) + \left(\frac{m_e - m_i}{\rho_s}\right)} \quad (3)$$

$$-[\ln(1 - V_p) + V_p + \chi V_p^2] = \rho_p V_s M_c^{-1} V_p^{1/3} \quad (4)$$

$$CD = \frac{1}{2M_c} \quad (5)$$

where V_p is the volume fraction of the polymer blend in the swollen composite, which is calculated based on the weights of the samples before (m_i) and after (m_e) the swelling process, presented in Section 2.4.3. It should be mentioned that the mass of the filler (m_f) was also involved in the calculation procedure of crosslink density (CD). The terms ρ_p and ρ_s are the SBR/BR blend and toluene densities with the values of 0.976 and 0.866 g/cm^3, respectively. Also, the term M_c indicates the physical crosslinking concentration and V_s with the value of 106.4 cm^3/mol is the molar volume of toluene. The Flory–Huggins interaction parameter (χ) between toluene and the polymer blend is also calculated using the following equations:[48,49]

$$\chi = \chi_\beta + \frac{V_s(\delta_s - \delta_p)^2}{RT} \quad (6)$$

$$\delta_p = \delta_1\varphi_1 + \delta_2\varphi_2 \quad (7)$$

where χ_β with the value of 0.34 ± 0.08[49] is the entropy contribution to the Flory–Huggins interaction parameter. The parameters δ_s = 18.35 (J/cm^3)$^{0.5}$, δ_1 = 17.04 (J/cm^3)$^{0.5}$, and δ_2 = 17.15 (J/cm^3)$^{0.5}$ are the toluene, SBR, and BR solubility parameters, respectively. The solubility parameter of the polymer blend (δ_p) was calculated to be 17.05 (J/cm^3)$^{0.5}$ according to eq 7 and the volume fractions (φ_i) of SBR and BR in the composites. The terms T and R indicate the temperature and gas constant (8.314 J/mol·K), respectively.

Furthermore, to measure the swelling level in the SBR/BR-Si_3N_4 samples, the swelling ration (S_r) was determined for all the samples via the following equation:[50]

$$S_r = \frac{m_e - m_i}{m_i} \quad (8)$$

The achieved CD and S_r values for all the SBR/BR-Si_3N_4 composites are shown together in Figure 4.

https://doi.org/10.1021/acsomega.3c03548
ACS Omega 2023, 8, 32701−32711

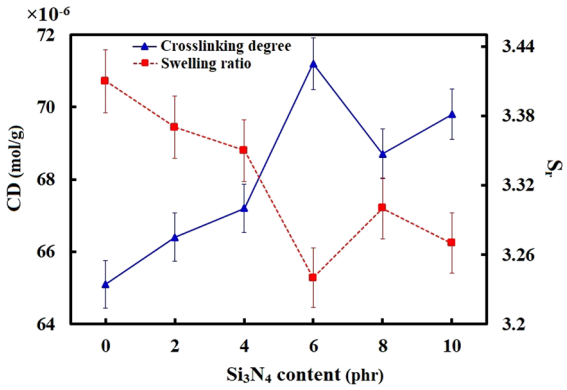

Figure 4. Crosslink density (CD) (calculated according to the FR equation) and swelling ratio (S_r) for the SBR/BR-Si_3N_4 samples as a function of the Si_3N_4 loading content.

According to Figure 4, increasing the amount of the Si_3N_4 filler in the SBR/BR-Si_3N_4 composite led to an enhancement of the crosslinking degree. The crosslink density reached the maximum value with the addition of 6 phr Si_3N_4 to the compound. It can be attributed to a more uniform heat distribution in the compound media during the curing process due to the presence of a highly thermally conductive filler in the polymer matrix, Si_3N_4.[50] This means that the presence of Si_3N_4 leads to more crosslinking reactions between the polymers chains, which results in a composite with a higher level of crosslinking. After the addition of 6 phr Si_3N_4, the crosslinking degree was significantly reduced due to Si_3N_4 agglomeration, although the further increment of the filler caused a higher value for CD. This is because the amount of Si_3N_4 in the composite at a higher level overcame the influence of Si_3N_4 agglomeration. In fact, this phenomenon is the main factor in the variations of the mechanical and physical properties of the SBR/BR-Si_3N_4 composite.

Moreover, as seen in Figure 4, a higher level of crosslinking degree led to a lower swelling ratio in the composite. This is because the higher crosslinks between the polymer chains prevented the network structure to swell. This behavior is so favorable for the tire industry, particularly in the part of the tire tread. Factually, it seems that the number of created covalent bonds to construct the network structure in the SBR/BR-Si_3N_4 composite is a function of the Si_3N_4 amount. According to the results, the highest amount of the crosslinking degree occurred in the S3 sample. However, the presence of Si_3N_4 in the composite improved the crosslinks between the polymer chains compared to the pure SBR/BR blend. Therefore, the SBR/BR-Si_3N_4 sample with the Si_3N_4 amount of 6 phr is a great candidate for tire tread.

3.4. Compression Properties. Compression set is one of the most important criteria to measure the returnability of rubbery composites to their original shape and size after being compressed.[51] According to the space bars (L_1), initial (L_0) and final (L_2) thicknesses of the samples (see Section 2.4.4), and the following equation,[52] the CS for all the composite samples was calculated and is reported in Figure 5.

$$\mathrm{CS}(\%) = \frac{L_0 - L_2}{L_0 - L_1} \times 100 \quad (9)$$

To find the relationship between the mechanical, microstructural, and physical properties of the SBR/BR-Si_3N_4 composite, the calculated toughness, crosslink density, and CS of the samples are exhibited together in Figure 5.

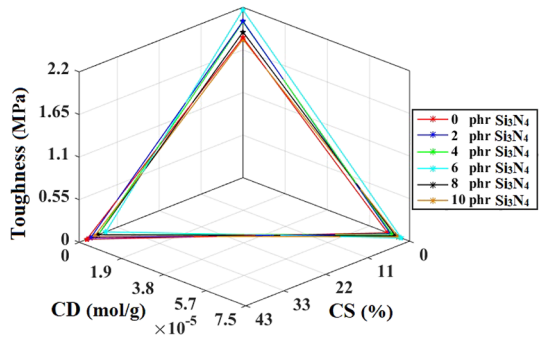

Figure 5. Three-dimensional figure of toughness-crosslink density (CD)−compression set (CS) as a function of Si_3N_4 loading content.

As seen in Figure 5, the CS amount of the composite was decreased with the Si_3N_4 loading content by 6 phr and, after that, the trend was changed. Hence, the composite containing the Si_3N_4 amount of 6 phr had the highest returnability, which is desirable for the tire industry. According to Figure 5, the highest amount of crosslinking degree led to the lowest amount of the CS and the furthest toughness for the composite. In fact, the presence of the Si_3N_4 filler in the composite, particularly at the loading content of 6 phr, caused a stronger network structure. Subsequently, when the pressure was removed from the composite sample, the rubber chains returned to their former positions more quickly than the other samples. This issue was the origin of the reduction of the CS in the composite with 6 phr of Si_3N_4. It should be noted that the agglomeration of the Si_3N_4 particles had an undesirable effect on the composite compression features, which caused to enhance the CS value at Si_3N_4 > 6 phr.

3.5. Physical Properties. Figure 6 illustrates the density and hardness (Shore A) of the cured SBR/BR-Si_3N_4 composite

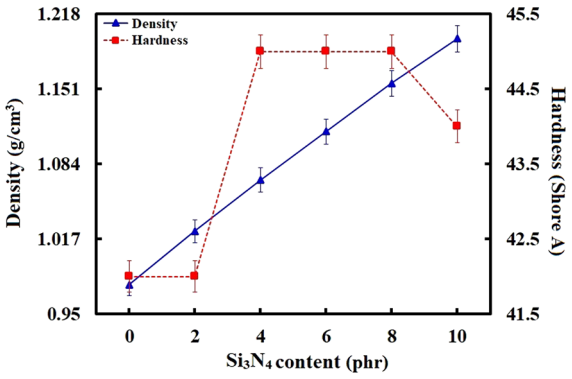

Figure 6. Density and hardness (Shore A) of the SBR/BR-Si_3N_4 samples as a function of the Si_3N_4 loading content.

as a function of Si_3N_4 content. As seen in the figure, the density of the samples was raised with the loading content of the Si_3N_4 filler, due to the high innate density of Si_3N_4.

Hardness is an important physical characteristic for a car tire, particularly the tread section, which is defined as the composite resistance to indentation.[53] Factually, the used durometer is an instrument that measures the penetration of a stress-loaded metal sphere into the SBR/BR-Si_3N_4 composite. As shown in Figure 6, there is a significant increase in hardness of the composite when the filler content increases to 4 phr.

https://doi.org/10.1021/acsomega.3c03548
ACS Omega 2023, 8, 32701−32711

This is because the increment of the filler in the composite media led to an enhancement of the crosslink density and also had a reinforcement impact on the polymer blend. However, more increment of the Si_3N_4 content to the range of 4−6 phr did not have any impact on the composite hardness. After this range, the hardness was decreased from 45 to 44 in Shore A because of the filler agglomeration. Generally, the reinforced SBR/BR-Si_3N_4 composite exhibited improved physical properties than the unfilled vulcanized SBR/BR.

3.6. Thermal Diffusivity. In this work, to evaluate the effect of Si_3N_4 on the thermal conductivity of SBR/BR-Si_3N_4, thermal diffusivity was determined for each sample at the temperature of 90 °C. The results are shown in Figure 7. As

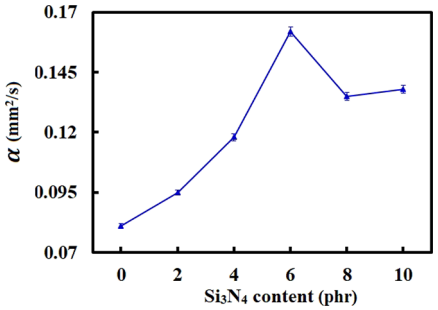

Figure 7. Thermal diffusivity (α) of SBR/BR-Si_3N_4 as a function of Si_3N_4 loading content at the temperature of 90 °C.

seen in the figure, the thermal diffusivity of the SBR/BR-Si_3N_4 composite was increased with increasing the filler content up to 6 phr. According to Figure 7, the presence of 6 phr Si_3N_4 in the compound led to an enhancement of the thermal diffusivity of the composite by ∼98%. This phenomenon is due to the highly thermally conductive innate density of Si_3N_4, 86−120 W/m·K.[36] The filler has helped to accelerate the heat transfer into the composite. After the optimum level of the filler (6 phr), the trend of the diagram was changed due to the filler agglomeration (see Figure 3). Indeed, manufacturing a tire with good thermal diffusivity has great importance. This is because the increment of heat transfer in the tire prevents the tire explosion while deriving due to the increment of air temperature within the tire, particularly in hot weather. Accordingly, the applied filler can be useful in the tire industry. Moreover, the results indicate that the presence of Si_3N_4 in the compound media can accelerate the vulcanization reaction because of increasing the thermal diffusivity in the compound.

3.7. Kinetics of Curing Reaction. In consideration of rubber, rheometry analysis is usually used to investigate the stiffness of a rubber during the vulcanization process. In fact, the rubber stiffness is an indicator of the curing degree of the rubber. In this work, rheometry evaluations were implemented on the SBR/BR-Si_3N_4 compounds during the curing process via obtaining the variations of the rheometer torque as a function of time. The torque−time curves for all the SBR/BR-Si_3N_4 samples as a function of Si_3N_4 loading content are presented in Figure 8. In the present work, Figure 8 is utilized to calculate the cure characteristics of the SBR/BR-Si_3N_4 compounds.

In order to determine the kinetic characteristics of curing reaction of the SBR/BR-Si_3N_4 compounds, the scorch (t_s) and optimum curing (t_{90}) times were computed, as shown in Figure 8. All the obtained cure times are exhibited together in Figure 9a.

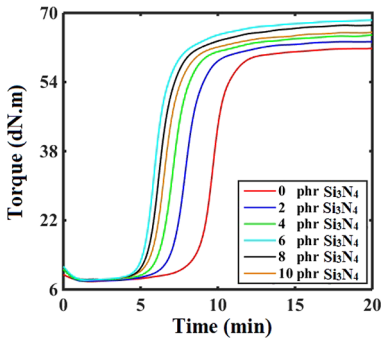

Figure 8. Torque−vulcanization time curve for the SBR/BR-Si_3N_4 compound as a function of the Si_3N_4 loading content during the curing process on ODR rheometry analysis.

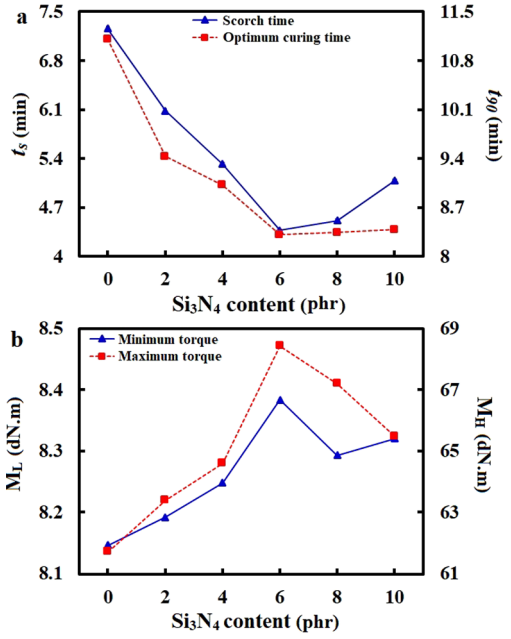

Figure 9. (a) Scorch (t_s) and optimum curing (t_{90}) times and (b) minimum (M_L) and maximum (M_H) torques for the SBR/BR-Si_3N_4 compound in the rheometry analysis versus the Si_3N_4 loading content extracted from Figure 8.

As seen in Figure 9a, there is a descendant trend of scorch and optimum curing times when the Si_3N_4 content is increased in the formulations. The furthest decrease occurred in the SBR/BR-Si_3N_4 compound with the Si_3N_4 loading content of 6 phr. This means that the presence of a highly thermally conductive filler of Si_3N_4 in the SBR/BR-Si_3N_4 compound had a catalytic effect on the curing reaction. This phenomenon led to acceleration in the vulcanization reaction of SBR/BR-Si_3N_4. Accordingly, among the different recipes, the compound containing 6 phr of Si_3N_4 had the fastest curing reaction, due to a better heat transfer in the polymer media resulted by the Si_3N_4 particles. According to Figure 9b, addition of the Si_3N_4 filler to the SBR/BR-Si_3N_4 compound not only reduced the curing times but also enhanced the variation of ODR torques. As seen in Figure 9b, the minimum (M_L) and maximum (M_H) torques detected during the rheometry test were increased with the Si_3N_4 loading content. This means that the added filler to the compound improved the curing rate of the compound and the crosslinking degree of the cured composite, particularly at 6 phr of Si_3N_4. According to Figure

https://doi.org/10.1021/acsomega.3c03548
ACS Omega 2023, 8, 32701−32711

9, the variation trend was changed after the filler amount of 6 phr. It can be attributed to the agglomeration of the filler particles followed by the reduction of the filler performance in the polymer matrix.

For more clarification regarding the effect of Si_3N_4 on the rate of the curing reaction of SBR/BR-Si_3N_4, the conversion of vulcanization reaction was also quantified. The conversion of curing reaction during the curing process was calculated using eq 1. The resultant data with respect to the time of rheometry test is shown in Figure 10.

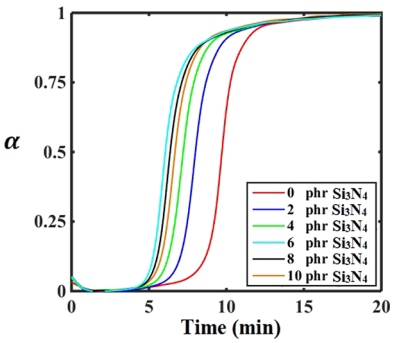

Figure 10. Conversion (α) of the curing reaction of the SBR/BR-Si_3N_4 compound as a functions of rheometry time and Si_3N_4 loading content.

As shown in Figure 10, the presence of the Si_3N_4 filler in the compound led to an increase in the conversion of the curing reaction of the SBR/BR-Si_3N_4 samples. Moreover, it helped to complete the curing process at the lower times. Therefore, the Si_3N_4 particles accelerated the curing reaction of the SBR/BR-Si_3N_4 compounds because of the increase in the heat distribution within the polymer bulk. As mentioned above, this phenomenon can be expressed by the catalytic effect of Si_3N_4 on the curing reaction of the compounds. In the investigation procedure of the kinetics of the vulcanization reaction of SBR/SBR-Si_3N_4, the conversion−time curves presented in Figure 10 are used as basic data.

Figure 11 shows the experimental values of curing reaction rate of the SBR/BR-Si_3N_4 compounds with the predicted values by the presented kinetic model in eq 2. The figure illustrates that the Kamal−Sourour kinetic model (modified by Ferasat et al.[41]) can predict the entire process of the curing reaction of SBR/BR-Si_3N_4 because of the *R*-squared value of $R^2 \sim 1$ in the fitting process. As seen in Figure 11, the maximum curing rate was increased with the Si_3N_4 loading content; however, the trend was changed after the Si_3N_4 content of 6 phr. Accordingly, the SBR/BR-Si_3N_4 compound with the filler content of 6 phr had the furthest curing rate compared to the other samples.

The achieved parameters of the kinetic model are listed in Table 2. Table 2 reveals that the addition of highly thermally conductive Si_3N_4 to the SBR/BR blend leads to change in the kinetic parameters of the curing reaction evidently.

This means that the filler causes a significant effect on the curing reaction of SBR/BR-Si_3N_4. According to the results listed in Table 2, the kinetic parameters obtained in the present work can be used to describe the kinetics of vulcanization reaction of SBR/BR-Si_3N_4 in the tire industry. These parameters can be helpful to determine the curing degree of SBR/BR-Si_3N_4 at certain amounts of the filler and time.

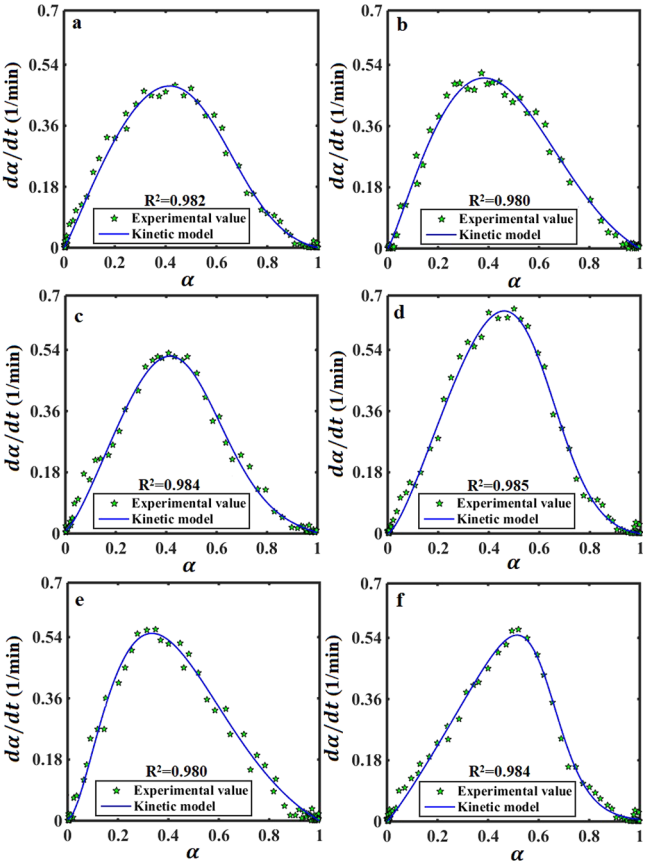

Figure 11. Experimental rate ($d\alpha/dt$) of the curing reaction of the SBR/BR-Si_3N_4 compound with the obtained kinetic model for the samples containing, (a) 0.0, (b) 2.0, (c) 4.0, (d) 6.0, (e) 8.0, and (f) 10.0 phr of Si_3N_4.

Furthermore, the maximum vulcanization rate $[d\alpha/dt]_{max}$—obtained from Figure 11—versus the Si_3N_4 content was calculated and is reported in Figure 12. As seen in the figure, the catalytic impact in SBR/BR-Si_3N_4 with the Si_3N_4 content of 6 phr is much further than the pure SBR/BR blend because of a better heat distribution of Si_3N_4 in the compound media. After this amount of filler, the catalytic impact of Si_3N_4 was reduced because of the filler agglomeration.

Therefore, the presented kinetic model has great importance from a practical point of view. According to the kinetic results, the Si_3N_4 content of 6 phr can be a good candidate to enhance the rate of the curing reaction of SBR/BR-Si_3N_4.

As seen in Figures 10−12, the addition of Si_3N_4 to the composite led to an acceleration of the curing reaction due to the filler catalytic effect on the vulcanization reaction. This issue caused the reaction conversion to reach its maximum amount rapidly at lower curing times with a higher vulcanization rate. The calculated kinetic parameters using the Kamal−Sourour-modified model can be helpful in the tire industry to predict the vulcanization characteristics in the composite manufacturing. Moreover, the obtained physical and mechanical properties showed that the compound with the maximum curing rate had the most improved tensile, compression, crosslink density, and microstructural, thermal, and physical properties, due to the best heat distribution and thermal diffusivity resulted by Si_3N_4.

https://doi.org/10.1021/acsomega.3c03548
ACS Omega 2023, 8, 32701−32711

Table 2. The Constants of the Kinetic Model for the Curing Reaction of the SBR/BR-Si_3N_4 Samples According to the Kamal–Sourour-Modified Model

sample code	k_1 (1/min)	k_2 (1/min)	C	m	n	$m + n$	α_c
S0	3.72×10^{-12}	2.329	10.13	1.103	0.89	1.993	0.711
S1	2.34×10^{-14}	3.968	4.395	1.205	0.91	2.115	0.524
S2	8.72×10^{-3}	3.233	8.325	1.366	0.586	1.952	0.533
S3	2.59×10^{-13}	4.391	10.13	1.471	0.647	2.118	0.647
S4	10.21×10^{-2}	4.594	4.048	1.841	0.997	2.838	0.641
S5	1.59×10^{-5}	1.363	14.72	1.121	0.870	1.991	0.633

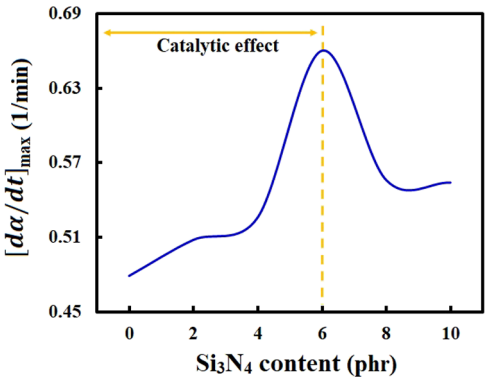

Figure 12. Effect of the Si_3N_4 loading content on the maximum vulcanization rate $[d\alpha/dt]_{max}$ of the SBR/BR-Si_3N_4 compound.

4. CONCLUSIONS

In this work, the effect of a highly thermally conductive filler, Si_3N_4, was studied on the mechanical, microstructural, and physical properties as well as the kinetics of vulcanization reaction of the SBR/BR-Si_3N_4 composite. It was found that the presence of Si_3N_4 in the composite media led to improvement in the tensile and compression properties of SBR/BR-Si_3N_4. The sample with the Si_3N_4 content of 6 phr had the most effect on the mechanical features of the composite (an increase of 1.14 and 1.2 times in the maximum strain and toughness, a smooth increase in TS as a 13% reduction in CS of the composite). Moreover, the calculated crosslink density using the Flory–Rehner equation through the swelling test clearly indicated that the presence of Si_3N_4 in the composite increased the covalent bonds between the polymer chains during the curing reaction. Among different formulations, the composite containing 6 phr Si_3N_4 led to the most increase of the crosslinking degree, from 6.51×10^{-5} to 7.12×10^{-5} mol/g. In addition, the rheometry results illustrated that the Si_3N_4 filler in the composite recipe decreased the scorch and optimum curing times by ∼40 and ∼25% compared to the sample without Si_3N_4, respectively. Moreover, an autocatalytic model based on the Kamal–Sourour model was applied to describe the kinetics of curing reaction of the compounds. The calculated kinetic parameters using the rheometry results indicated that the presence of a highly thermally conductive filler within the SBR/BR-based compounds led to a change in the kinetic parameters. According to the obtained kinetic characteristics, it can be concluded that the Si_3N_4 particles accelerated the curing reaction, because of enhancement in heat transfer into the compound during the vulcanization reaction, particularly at 6 phr; however, after that, the trend was changed. This issue can help to reduce the required amount of energy consumption in the tire industry to cure the tire tread. According to the results, it seems that the composite including 6 phr of Si_3N_4 is a good candidate for tire tread. This is because it leads to improvement in the mechanical, microstructural, physical, and kinetic features of the composite.

AUTHOR INFORMATION

Corresponding Author

Mohammad Fasihi − *School of Chemical, Petroleum and Gas Engineering, Iran University of Science and Technology (IUST), 13114 Tehran, Iran;* orcid.org/0000-0003-0362-118X; Email: mfasihi@iust.ac.ir

Authors

Sajad Rasouli − *School of Chemistry, Iran University of Science and Technology (IUST), 3319613111 Tehran, Iran*

Amirreza Zabihi − *Compounding Laboratory, Department of Technology, Kian Tire Manufacturing Company, Tehran 401310, Iran*

Gholamreza Bozorg Panah Kharat − *Compounding Laboratory, Department of Technology, Kian Tire Manufacturing Company, Tehran 401310, Iran*

Complete contact information is available at: https://pubs.acs.org/10.1021/acsomega.3c03548

Notes

The authors declare no competing financial interest.

ACKNOWLEDGMENTS

The authors would like to thank Kian Tire Manufacturing Company for providing raw materials and some measuring equipment for this study.

REFERENCES

(1) Saini, A.; Unnikrishnakurup, S.; Krishnamurthy, C.-V.; Balasubramanian, K.; Sundararajan, T. Numerical study using finite element method for heat conduction on heterogeneous materials with varying volume fraction, shape and size of fillers. *Int. J. Therm. Sci.* **2021**, *159*, No. 106545.

(2) Yang, D.; Yu, L.; Liang, Y.; Wei, Q.; Ni, Y.; Zhang, L. Enhanced Electromechanical Performance of Natural Rubber Composites via Constructing Strawberry-like Dielectric Nanoparticles. *ACS Appl. Polym. Mater.* **2020**, *2*, 5621−5629.

(3) Marín-Genescà, M.; García-Amorós, J.; Mudarra, J.; Vidal, L. M.; Cañavate, J.; Colom, X. Insights into the Structural and Dielectric Behavior of Composites Produced from EPDM Waste Processed through a Devulcanization Method and SBR. *ACS Omega* **2023**, *8*, 12830−12841.

(4) Thomas, R.-M.; Lightbown, I.-E.; Sparks, W.-J.; Frolich, P.-K.; Murphree, E.-V. Butyl Rubber a New Hydrocarbon Product. *Ind. Eng. Chem.* **1940**, *32*, 1283−1292.

(5) Caradant, L.; Lepage, D.; Nicolle, P.; Prébé, A.; Aymé-Perrot, D.; Dollé, M. Effect of Li^+ Affinity on Ionic Conductivities in Melt-Blended Nitrile Rubber/Polyether. *ACS Appl. Polym. Mater.* **2020**, *2*, 4943−4951.

(6) Xiang, H.-P.; Rong, M.-Z.; Zhang, M.-Q. Self-healing, Reshaping, and Recycling of Vulcanized Chloroprene Rubber: A Case Study of Multitask Cyclic Utilization of Cross-linked Polymer. *ACS Sustainable Chem. Eng.* **2016**, *4*, 2715−2724.
(7) Yu, S.; Zuo, H.; Xu, X.; Ning, N.; Yu, B.; Zhang, L.; Tian, M. Self-Healable Silicone Elastomer Based on the Synergistic Effect of the Coordination and Ionic Bonds. *ACS Appl. Polym. Mater.* **2021**, *3*, 2667−2677.
(8) De, S.-K.; White, J.-R., *Rubber Technologist's Handbook*, iSmithers Rapra Publishing, 2001. ISBN: 1859572626
(9) Kumar, S.; Chattopadhyay, S.; Sreejesh, A.; Nair, S.; Unnikrishnan, G.; Nando, G.-B. Analysis of air permeability and WVTR characteristics of highly impermeable novel rubber nanocomposite. *Mater. Res. Express* **2015**, *2*, No. 025001.
(10) Vega-Cantú, Y.; Hauge, R.; Norman, L.; Billups, W.-E. Enhancement of the chemical resistance of nitrile rubber by direct fluorination. *J. Appl. Polym. Sci.* **2003**, *89*, 971−979.
(11) Kang, J.; Zhang, B.; Li, G. The abrasion-resistance investigation of rubberized concrete. *J. Wuhan Univ. Technol.-Mat. Sci. Edit.* **2012**, *27*, 1144−1148.
(12) Ruellan, B.; Le Cam, J.-B.; Jeanneau, I.; Canévet, F.; Mortier, F.; Robin, E. Fatigue of natural rubber under different temperatures. *Int. J. Fatigue* **2019**, *124*, 544−557.
(13) Niu, H.; Ren, Y.; Guo, H.; Małycha, K.; Orzechowski, K.; Bai, S.-L. Recent progress on thermally conductive and electrical insulating rubber composites: Design, processing and applications. *Composites Commun.* **2020**, *22*, No. 100430.
(14) Sharma, G.; Khanduja, R. Performance evaluation and availability analysis of feeding system in a sugar industry. *Int. J. Res. Eng. Appl. Sci.* **2013**, *3*, 38−50.
(15) Evans, M.-S.; *Tyre Compounding for Improved Performance*, Volume *12*, iSmithers Rapra Publishing, 2002. ISBN: 1859573061
(16) Li, J.; Zheng, D.; Yao, Z.; Wang, S.; Xu, R.; Deng, S.; Wang, J. Formation Mechanism of Monocyclic Aromatic Hydrocarbons during Pyrolysis of Styrene Butadiene Rubber in Waste Passenger Car Tires. *ACS Omega* **2022**, *7*, 42890−42900.
(17) Sae-oui, P.; Suchiva, K.; Sirisinha, C.; Intiya, W.; Yodjun, P.; Thepsuwan, U. Effects of Blend Ratio and SBR Type on Properties of Carbon Black-Filled and Silica-Filled SBR/BR Tire Tread Compounds. *Adv. Mater. Sci. Eng.* **2017**, 2476101.
(18) Martín-Martínez, J.-M.; Chapter 13 - Rubber base adhesives, *Adhesion Science Engineering*, Elsevier Science B.V., 2002, 573−675, DOI: 10.1016/B978-044451140-9/50013-5.
(19) Kang, C.-H.; Kim, M.-S. Tread rubber composition and tire manufactured by using the same. *Kor. Pat.* **2013**, 10-2013-0071620.
(20) Marzocca, A.-J.; Cerveny, S.; Méndez, J.-M. some considerations concerning the dynamic mechanical properties of cured styrene−butadiene rubber/polybutadiene blends. *Polym. Int.* **2000**, *49*, 216−222.
(21) Jin, J.; Noordermeer, J. W. M.; Blume, A.; Dierkes, W. K. Effect of SBR/BR elastomer blend ratio on filler and vulcanization characteristics of silica filled tire tread compounds. *Polym. Test.* **2021**, *99*, No. 107212.
(22) An, D.; Cheng, S.; Jiang, C.; Duan, X.; Yang, B.; Zhang, Z.; Li, J.; Liu, T.; Wong, C. A novel environmentally friendly boron nitride/lignosulfonate/natural rubber composite with improved thermal conductivity. *J. Mater. Chem. C* **2020**, *8*, 4801−4809.
(23) Shiva, M.; Akhtari, S.-S.; Shayesteh, M. Effect of mineral fillers on physico-mechanical properties and heat conductivity of carbon black-filled SBR/butadiene rubber composite. *Iran. Polym. J.* **2020**, *29*, 957−974.
(24) An, D.; Duan, X.; Cheng, S.; Zhang, Z.; Yang, B.; Lian, Q.; Li, J.; Sun, Z.; Liu, Y.; Wong, C.-P. Enhanced thermal conductivity of natural rubber based thermal interfacial materials by constructing covalent bonds and three-dimensional networks. *Composites, Part A* **2020**, *135*, No. 105928.
(25) Akshay, K.; Arjun, M.; Govind, S. S.; Hrithwik, V.; Rahulan, N. Mechanical behavior of silicon carbide filled SBR/NBR blends. *Mater. Today Proc.* **2021**, *42*, 1432−1436.
(26) Wu, J.; Song, X.; Gong, Y.; Yang, W.; Chen, L.; He, S.; Lin, J.; Bian, X. Analysis of the heat conduction mechanism for Al2O3/Silicone rubber composite material with FEM based on experiment observations. *Compos. Sci. Technol.* **2021**, *210*, No. 108809.
(27) Qu, J.; Fun, L.; Mukerabigwi, J.-F.; Liu, C.; Cao, Y. A silicon rubber composite with enhanced thermal conductivity and mechanical properties based on nanodiamond and boron nitride fillers. *Polym. Compos.* **2021**, *42*, 4390−4396.
(28) Ma, A.; Chen, W.; Hou, Y.; Zhang, G. The Preparation and Cure Kinetics Researches of Thermal Conductivity Epoxy/AlN Composites. *Polym.-Plast. Technol. Eng.* **2010**, *49*, 354−358.
(29) Andideh, M.; Ghoreishy, M.-H.-R.; Soltani, S.; Sourki, F.-A. Surface modification of oxidized carbon fibers by grafting bis-(triethoxysilylpropyl) tetrasulfide (TESPT) and rubber sizing agent: Application to short carbon fibers/SBR composites. *Composites, Part A* **2021**, *141*, No. 106201.
(30) Dugast, G.; Settar, A.; Chetehouna, K.; Gascoin, N.; Marceau, J.-L.; Bouchez, M.; De Bats, M. Experimental and numerical analysis on the thermal degradation of reinforced silicone-based composites: Effect of carbon fibres and silicon carbide powder contents. *Thermochim. Acta* **2020**, *686*, No. 178563.
(31) Huang, X.; Jiang, P.; Tanaka, T. A review of dielectric polymer composites with high thermal conductivity. *IEEE Electr. Insul. Mag.* **2011**, *27*, 8−16.
(32) Xia, R.; Zhang, Y.; Zhu, Q.; Qian, J.; Dong, Q.; Li, F. Surface modification of nano-sized silicon nitride with BA-MAA-AN tercopolymer. *J. Appl. Polym. Sci.* **2008**, *107*, 562−570.
(33) Belgacemi, R.; Derradji, M.; Trache, D.; Zegaoui, A.; Mehelli, O.; Tarchoun, A. F. Advanced hybrid materials from epoxy, oxidized UHMWPE fibers and silane surface modified silicon nitride nanoparticles. *High Perform. Polym.* **2021**, *33*, 440−450.
(34) Tai, Y.-L.; Qian, J.-S.; Miao, J.-B.; Xia, R.; Zhang, Y.-C.; Yang, Z.-G. Preparation and characterization of Si3N4/SBR nanocomposites with high performance. *Mater. Des.* **2012**, *34*, 522−527.
(35) Derradji, M.; Ramdani, N.; Zhang, T.; Wang, J.; Lin, Z.-W.; Yang, M.; Xu, X.-D.; Liu, W.-B. High thermal and thermomechanical properties obtained by reinforcing a bisphenol-A based phthalonitrile resin with silicon nitride nanoparticles. *Mater. Lett.* **2015**, *149*, 81−84.
(36) Ramdani, N.; Derradji, M.; Feng, T.-T.; Tong, Z.; Wang, J.; Mokhnache, E.-O.; Liu, W.-B. Preparation and characterization of thermally-conductive silane-treated silicon nitride filled polybenzoxazine nanocomposites. *Mater. Lett.* **2015**, *155*, 34−37.
(37) Hands, D.; Horsfall, F. The thermal diffusivity and conductivity of natural rubber compounds. *Rubber Chem. Technol.* **1977**, *50*, 253−265.
(38) Goyanes, S.; Lopez, C.-C.; Rubiolo, G.-H.; Quasso, F.; Marzocca, A.-J. Thermal properties in cured natural rubber/styrene butadiene rubber blends. *Eur. Polym. J.* **2008**, *44*, 1525−1534.
(39) Marzocca, A.-J.; Mansilla, M.-A. Vulcanization kinetic of styrene−butadiene rubber by sulfur/TBBS. *J. Appl. Polym. Sci.* **2006**, *101*, 35−41.
(40) Arrillaga, A.; Zaldua, A. M.; Atxurra, R. M.; Farid, A. S. Techniques used for determining cure kinetics of rubber compound. *Eur. Polym. J.* **2007**, *43*, 4783−4799.
(41) Ferasat, H.; Fasihi, M.; Ghoreishy, M.-H.-R.; Ajorloo, M. Development of a bubble growth model for natural rubber-based foams. *Polym. Eng. Sci.* **2020**, *61*, 477−488.
(42) Sanctuary, R.; Baller, J.; Zielinski, B.; Becker, N.; Krüger, J.-K.; Philipp, M.; Müller, U.; Ziehmer, M. Influence of Al2O3 nanoparticles on the isothermal cure of an epoxy resin. *J. Phys. Condens. Matter* **2009**, *21*, No. 035118.
(43) Promsung, R.; Nakaramontri, Y.; Uthaipan, N.; Kummerlöwe, C.; Johns, J.; Vennemann, N.; Kalkornsurapranee, E. Effects of Protein Contents in Different Natural Rubber Latex Forms on the Properties of Natural Rubber Vulcanized with Glutaraldehyde. *Express Polym. Lett.* **2021**, *15*, 308−318.
(44) Phomrak, S.; Nimpaiboon, A.; Newby, B.-M. Z.; Phisalaphong, M. Natural Rubber Latex Foam Reinforced with Micro-and

Nanofibrillated Cellulose via Dunlop Method. *Polymer* **2020**, *12*, 1959.
(45) Rasouli, S.; Raveshtian, A.; Fasihi, M. Thermal Characteristics, Kinetics and Thermodynamics of Thermal Degradation Reaction, and Hydrophobicity of Corn Starch Affected by Chemical and Physical Modifications. *Starch* **2022**, *74*, 2100185.
(46) Ariff, Z.-M.; Zakaria, Z.; Tay, L.-H.; Lee, S.-Y. Effect of Foaming Temperature and Rubber Grades on Properties of Natural Rubber Foams. *J. Appl. Polym. Sci.* **2008**, *107*, 2531−2538.
(47) Raveshtian, A.; Fasihi, M.; Norouzbeigi, R.; Rasouli, S. The influence of Dunlop and air microbubbling manufacturing methods on the physical, microstructural and mechanical properties of nano-alumina filled natural rubber latex foam. *Express Polym. Lett.* **2022**, *16*, 649−664.
(48) Rasouli, S.; Moghbeli, M.-R.; Nikkhah, S.-J. A deep insight into the polystyrene chain in cyclohexane at theta temperature: molecular dynamics simulation and quantum chemical calculations. *J. Mol. Model.* **2019**, *25*, 195.
(49) Sperling, L.-H.; *Introduction to physical polymer science*, (4th ed.), Wiley: New York, 2005.
(50) Wong, K. V.; Kurma, T. Transport Properties of Alumina NanoFluid. *Nanotechnology* **2008**, *19*, No. 345702.
(51) Ramli, R.; Chai, A. B.; Ho, J. H.; Kamaruddin, S.; Rasdi, F. R.; De Focatiis, D. S. A. Specialty Natural Rubber Latex Foam: Foamability Study and Fabrication Process. *Rubber Chem. Technol.* **2022**, *95*, 492−513.
(52) Bashir, A. S. M.; Manusamy, Y.; Chew, T. L.; Ismail, H.; Ramasamy, S. Mechanical, Thermal, and Morphological Properties of (Eggshell Powder)-Filled Natural Rubber Latex Foam. *J. Vinyl Addit. Technol.* **2017**, *23*, 3−12.
(53) Vieira, T.; Lundberg, J.; Eriksson, O. Evaluation of uncertainty on Shore hardness measurements of tyre treads and implications to tyre/road noise measurements with the Close Proximity method. *Measurement* **2020**, *162*, No. 107882.

https://doi.org/10.1021/acsomega.3c03548
ACS Omega 2023, 8, 32701−32711